Polymer Journal (2014) 46, 728–735
© 2014 The Society of Polymer Science, Japan (SPSJ) All rights reserved 0032-3896/14
www.nature.com/pj

ORIGINAL ARTICLE

Trehalose-incorporated polymer network by thiol-ene photopolymerization

Shohei Nagashima, Toshiaki Shimasaki, Naozumi Teramoto and Mitsuhiro Shibata

Allyl-etherified trehalose (A*x*T), with a degree of allylation $x = 6$ or 8, was synthesized by the reaction of α,α-D-trehalose and allyl bromide at a feed molar ratio of 1:1.1*x*. The degrees of allylation measured by a proton nuclear magnetic resonance (^{1}H-NMR) method for A6T and A8T were 5.99 and 7.51, respectively. Thiol-ene photopolymerizations of A*x*T with pentaerythritol-based tetrathiol (S4P) and isocyanurate-based trithiol (S3I) produced trehalose-incorporated polymer networks (A*x*T-S4P and A*x*T-S3I). All of the photo-cured films exhibited high transparency to visible light. The tan δ peak temperatures of A8T-S4P and A6T-S4P (36.7 °C and 36.8 °C, respectively) were higher than those of A8T-S3I and A6T-S3I (21.9 °C and 23.2 °C, respectively). The former S4P-based film demonstrated much higher tensile strength and modulus at room temperature than the latter S3I-based film did. The 5% weight loss temperature of the A8T-based film was higher than that of the A6T-based film.
Polymer Journal (2014) **46,** 728–735; doi:10.1038/pj.2014.53; published online 2 July 2014

INTRODUCTION

Trehalose (α,α-D-trehalose) is a nonreducing disaccharide that is widely found in organisms, and it has important roles in biopreservation.[1–5] Since Hayashibara established an inexpensive production method for generating trehalose using an enzymatic reaction of starch,[6] production costs have been greatly reduced, and the applications for the material have been consequently extended. Trehalose is more stable against acid and heat than other reducing disaccharides, such as cellobiose and maltose. Additionally, this monomer possesses a symmetrical structure, which can allow the generation of a high-molecular-weight polymer or homogeneous polymer network, in contrast to sucrose, which is an asymmetric nonreducing disaccharide. Therefore, trehalose is a feasible starting disaccharide for the preparation of biobased polymers with high biocompatibility and biodegradability. In previous studies, trehalose was converted to linear polymers using acetalization reactions with dialdehyde compounds[7,8] and 'click' reactions, such as hydrosilylation,[9] Diels-Alder[10] and azide–acetylene coupling reactions.[11,12] Additionally, trehalose was converted to crosslinked polymers by vinylbenzyl etherification and subsequent thermal curing reactions.[13]

Recently, light-induced, radical-mediated thiol-ene 'click' reactions have attracted increasing attention as a method for the production of crosslinked polymer networks with various frameworks and functional groups.[14–18] Thiol-ene photopolymerization is characterized by advantages such as an inherently rapid reaction rate, reduced oxygen inhibition, high regioselectivity and low polymerization shrinkage. Furthermore, as the reaction is initiated by the formation of primary radicals by the photolysis of a photoinitiator and subsequent production of a thiyl radical by the abstraction of a hydrogen radical from the thiol group, monomers containing functional groups (OH, CO_2H, NH_2, etc.) with a hydrogen that is less easily abstracted than the hydrogen of a thiol group can be polymerized without protecting the functional groups. The thiol-ene photopolymerization is a promising curing reaction for the production of saccharide-incorporated polymer networks. Recently, Ortiz *et al.*[19,20] reported the dynamic mechanical properties and thermal stability of polymer networks prepared by the thiol-ene photopolymerization of allyl-etherified sucrose, with an allylation degree of ca. 2 (from 1 to 3), and polythiol compounds. In general, as thiol-ene networks are comprised of flexible sulfide bonds, their mechanical and thermal properties are inferior to those of conventional photo-cured resins, such as acrylate, methacrylate and epoxy resins.[21] Therefore, the properties of polymer networks generated by the thiol-ene photopolymerization of allyl-etherified disaccharides with higher degrees of allylation are an interesting subject.

The present study describes the properties of biobased polymer networks synthesized by the thiol-ene photopolymerization of allyl-etherified trehalose (A*x*T) with an allylation degree (x) higher than 3 ($3 < x \leq 8$). Our attention was focused on the influence of differences in the A*x*T allylation degree ($x = 6$ or 8) and of the polythiol compounds' framework structure on the thermal and mechanical properties of the polymer networks produced by thiol-ene photopolymerization (Figure 1).

Department of Life and Environmental Sciences, Faculty of Engineering, Chiba Institute of Technology, Chiba, Japan
Correspondence: Professor M Shibata, Department of Life and Environmental Sciences, Faculty of Engineering, Chiba Institute of Technology, 2-17-1, Tsudanuma, Narashino, Chiba 275-0016, Japan.
E-mail: mitsuhiro.shibata@p.chibakoudai.jp
Received 12 April 2014; revised 9 May 2014; accepted 12 May 2014; published online 2 July 2014

EXPERIMENTAL PROCEDURE

Materials

α,α-D-Trehalose dihydrate was kindly provided by Hayashibara (Okayama, Japan) and was dehydrated at 130 °C for 24 h before use. Pentaerythritol-based tetrathiol (S4P, substance name: pentaerythritol tetrakis(3-mercaptobutyrate), trade name: Karenz MT PE1) and isocyanurate-based trithiol (S3I, substance name: 1,3,5-tris(3-mercaptobutyryloxyethyl)-1,3,5-triazine-2,4,6(1*H*,3*H*,5*H*)-trione, trade name: Karenz MT NR1) were kindly provided by Showa Denko KK (Tokyo, Japan). The structures of S4P and S3I are shown in Figure 1. The photo-initiator 2-hydroxy-1-[4-(2-hydroxyethoxy)phenyl]-2-methyl-1-propanone (Irgacure 2959, mp. 86.5–89.5 °C, ultraviolet–visible absorption peak in methanol: 276 nm) was kindly provided by Ciba Specialty Chemicals KK (Tokyo, Japan). Allyl bromide, sodium hydroxide and dimethyl sulfoxide (DMSO) were purchased from Kanto Chemical (Tokyo, Japan). All of the commercially available reagents were used without further purification.

Preparation of A*x*T

The synthetic scheme for A*x*T is also shown in Figure 1. To a solution of dried trehalose (4.28 g, 12.5 mmol) in DMSO (150 ml), pulverized sodium hydroxide (8.00 g, 200 mmol) was added, and the mixture was stirred for 10 min. To the mixture, allyl bromide (13.3 g, 110 mmol) was added dropwise over a period of 30 min at room temperature, and then the mixture was stirred at room temperature for 24 h. The reaction mixture was filtered, poured into dilute hydrochloric acid and extracted with ethyl acetate. The organic layer was washed two times with water, dried over sodium sulfate and concentrated *in vacuo* to produce A8T as a yellow liquid (5.80 g) in a 70.0% yield.

In a similar manner, A6T (3.65 g) was synthesized using dried trehalose (4.28 g, 12.5 mmol), sodium hydroxide (6.00 g, 150 mmol) and allyl bromide (9.97 g, 82.5 mmol) at a 50.1% yield.

Thiol-ene photopolymerization of A*x*T and S4P

A mixture of A8T (1.72 g, 2.60 mmol), S4P (2.83 g, 5.19 mmol), Irgacure 2959 (136 mg, 0.693 mmol) and acetone (5 ml) was stirred for 30 min to form a homogeneous solution. The solution was poured on a poly(tetrafluoroethylene) culture dish with a diameter of 95 mm and was dried at 60 °C for 3 h. The obtained mixture was photo-irradiated for 15 s × 3 times at 1-min intervals to yield a photo-cured A8T/S4P (A8T-S4P) film (thickness: ca. 0.5 mm). A SPOT-CURE SP-7 (250 W light source, wavelength 240–440 nm; Ushio, Yokohama, Japan) device equipped with a uniform-radiation optical unit was used for ultraviolet curing (irradiation distance 200 mm, irradiation intensity 72 mW cm^{-2}). In a similar manner, photo-cured A6T/S4P (A6T-S4P) film (thickness: ca. 0.5 mm) was prepared using A6T (1.88 g, 3.24 mmol) and S4P (2.63 g, 4.82 mmol).

Thiol-ene photopolymerization of A*x*T and S3I

A mixture of A8T (1.37 g, 2.07 mmol), S3I (3.13 g, 5.51 mmol), Irgacure 2959 (135 mg, 0.688 mmol) and acetone (5 ml) was stirred for 30 min to produce a homogeneous solution. The solution was poured on a poly(tetrafluoroethylene) culture dish with a diameter of 95 mm and was dried at 60 °C for 3 h. The obtained mixture was photo-irradiated using the same conditions as those used during the preparation of A8T-S4P to yield a photo-cured A8T/S3I (A8T-S3I) film (thickness: ca. 0.5 mm). In a similar manner, photo-cured A6T/S3I (A6T-S3I) film (thickness: ca. 0.5 mm) was prepared using A6T (1.51 g, 2.59 mmol) and S3I (2.94 g, 5.18 mmol).

Measurements

Proton and carbon nuclear magnetic resonance (^{1}H- and ^{13}C-NMR) spectra were recorded on a Bruker AV-400 (400 MHz) (Bruker, Madison, WI, USA) using $CDCl_3$ as a solvent. Fourier transform infrared spectra were recorded on a Shimadzu FT-IR 8100 (Shimadzu, Kyoto, Japan) by the KBr pellet or attenuated

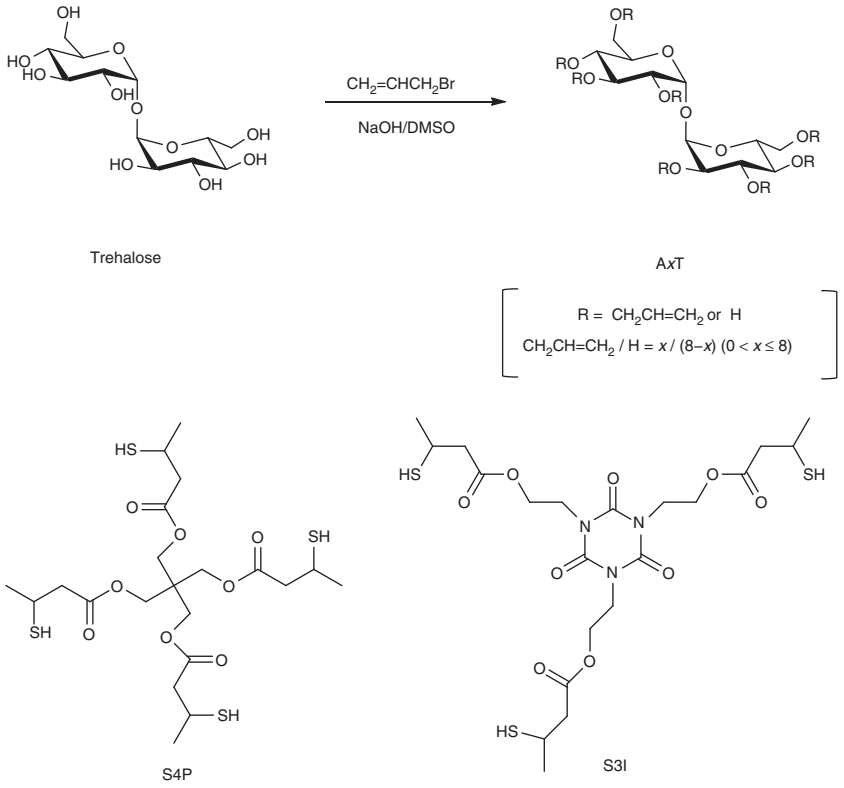

Figure 1 Synthetic scheme for allyl-etherified trehalose (A*x*T), and the structure of pentaerythritol-based tetrathiol (S4P) and isocyanurate-based trithiol (S3I).

total reflectance method. Ultraviolet–visible spectra were recorded on a JASCO V-650 instrument (JASCO, Tokyo, Japan) over the wavelength range of 400–800 nm using films with thicknesses of approximately 0.5 mm. Matrix-assisted laser desorption ionization time-of-flight mass spectrometry (MALDI-TOF MS) was performed on a Shimadzu KOMPACT Probe (Shimadzu) in a linear positive ion mode, using α-cyano-4-hydroxycinnamic acid (CHCA) as the matrix and acetonitrile/water (65/35) as the solvent. The differential scanning calorimetry (DSC) measurements were performed on a Perkin-Elmer Diamond DSC (Perkin-Elmer, Waltham, MA, USA) in a helium atmosphere. To eliminate the thermal history of the samples (8–12 mg), the samples were heated from −100 °C to 100 °C at a heating rate of 20 °C min^{-1}, held at the temperature for 3 min and then cooled to −100 °C at a cooling rate of 100 °C min^{-1}. After the temperature was held at −100 °C for 3 min, the second heating scan was performed at a heating rate of 20 °C min^{-1} to determine the glass transition temperature (T_g). Dynamic mechanical analysis (DMA) of the rectangular specimen (length 30 mm, width 5 mm, thickness 0.5 mm) was performed on a Rheolograph Solid (Toyo Seiki, Tokyo, Japan) with a chuck distance of 20 mm, a frequency of 1 Hz and a heating rate of 2 °C min^{-1}. The 5% weight loss temperature (T_5) was measured on a Shimadzu TGA-50 thermogravimetric analyzer (Shimadzu) at a heating rate of 20 °C min^{-1} in a nitrogen atmosphere. Tensile testing of the rectangular plates (length 50 mm, width 10 mm, thickness 0.5 mm) was performed at room temperature using an Autograph AG-1 (Shimadzu) based on the standard method for testing the tensile properties of plastics (JIS K7161:1994, ISO527-1). The span length was 25 mm, and the testing speed was 10 mm min^{-1}. Five specimens were tested for each set of samples. The mean values were calculated, and the differences between maximal and minimal values are displayed as error bars in the graphs.

RESULTS AND DISCUSSION

Characterization of A*x*T

A6T (or A8T) was synthesized by the reaction of trehalose and allyl bromide at the feed molar ratio of 1:6.6 (or 1:8.8) in the presence of excess pulverized sodium hydroxide in DMSO (Figure 1). Figure 2 shows the ^{1}H-NMR spectra of trehalose and A*x*T ($x = 6$ or 8) in d_6-DMSO and $CDCl_3$, respectively. The ^{1}H assignment for trehalose was performed according to the references[22–24] as follows: δ 4.89 (H-1), 4.70 (OH-3,4), 4.58 (OH-2), 3.42 (OH-6), 3.65 (H-5), 3.57 (H-3, 6), 3.49 (H-6), 3.25 (H-2) and 3.16 p.p.m. (H-4). The ^{1}H assignment for A8T was implemented using the ^{1}H assignments of trehalose and 3-propoxypropene (Website SDBS/RIO-DB/AIST). The olefinic ^{1}H signals of the allyl groups for A8T were observed at 5.91 (H-2′), 5.28 (H-3′a) and 5.15 p.p.m. (H-3′b). The methylene ^{1}H signals (H-1′a, 1′b) of the allyl groups for A8T were observed at 4.32 and 4.10 p.p.m. However, the peaks at 5.15 and 4.10 p.p.m. overlapped with other ^{1}H signals of the trehalose framework, judging from the ^{1}H integral values. As we could not specifically assign the ^{1}H signals of the trehalose framework of A8T, the two-dimensional NMR spectrum of A8T in $CDCl_3$ was obtained. Figure 3 shows the two-dimensional NMR spectrum of A8T obtained by C-H correlated spectroscopy. The olefinic carbons (C-2′and C-3′) of A8T were observed at 135.6, 135.2, 134.9, 134.8 p.p.m. and 117.2, 116.9, 116.8, 116.1 p.p.m., respectively. Their ^{13}C signals reasonably correlated to the ^{1}H-signals of H-2′ and H-3′a, 3′b, respectively. The acetal methine carbon (C-1) of A8T was

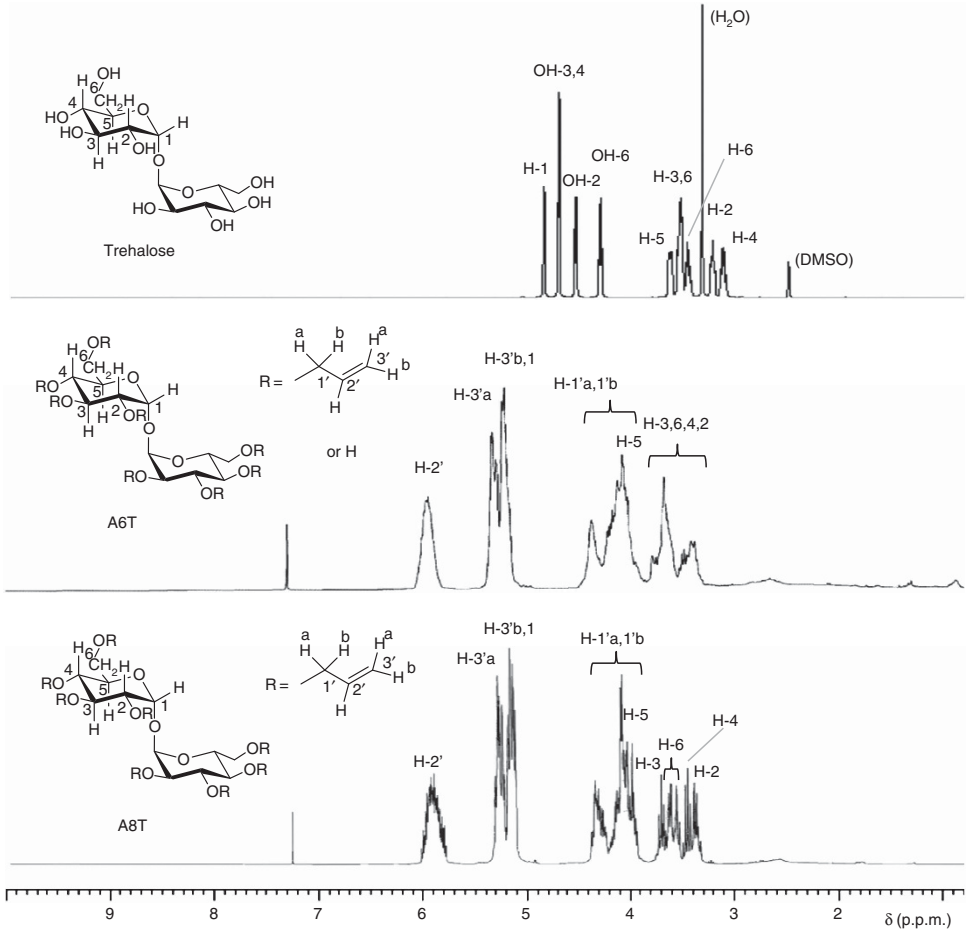

Figure 2 Proton nuclear magnetic resonance (^{1}H-NMR) spectra of trehalose in d_6-dimethyl sulfoxide (DMSO), A6T in $CDCl_3$ and A8T in $CDCl_3$.

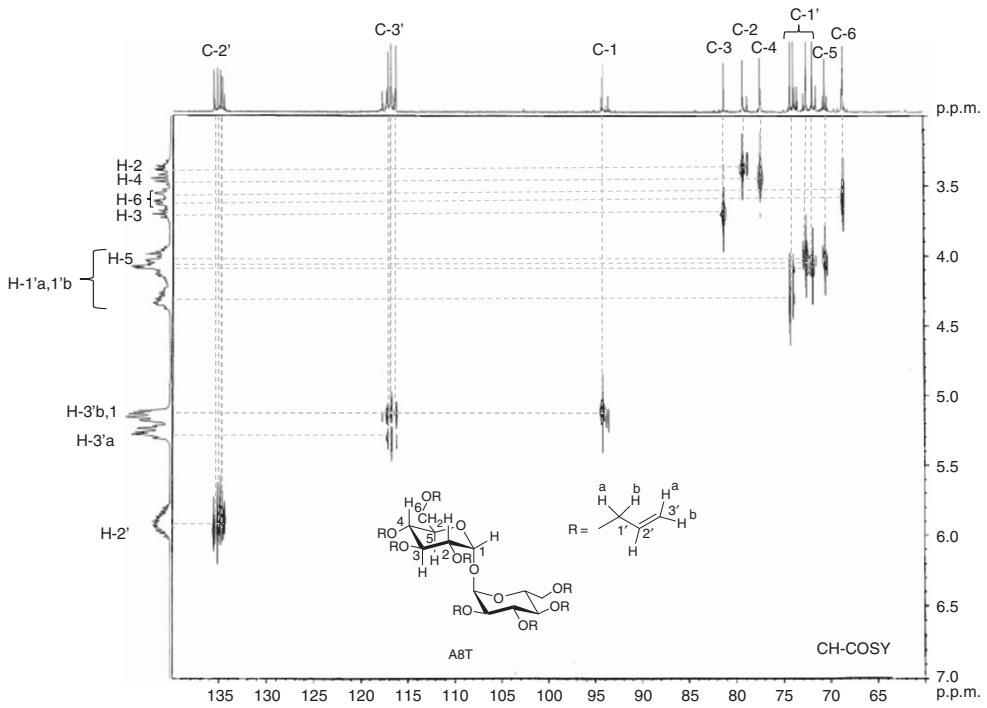

Figure 3 Two-dimensional C-H correlated spectroscopy (2D CH-COSY) spectrum of A8T in $CDCl_3$.

observed at the lowest magnetic field (94.2 p.p.m.) among the carbons of the trehalose framework. The C-1 signal was clearly correlated to the H-1 signal at 5.15 p.p.m. Therefore, we determined that the ^{1}H signal overlapping with H-3′b at 5.15 p.p.m. was H-1. Although the figures are not shown, we performed distortionless enhancement by polarization transfer experiments to discriminate between methine and methylene carbons. As a result, the ^{13}C signals at 74.2, 73.9, 72.8, 72.0 and 68.8 p.p.m. were determined to be methylene carbons. Among the ^{13}C signals, the signal at the highest magnetic field (68.8 p.p.m.) was reasonably assigned to C-6. The ^{1}H signal at 3.63 p.p.m. was assigned to H-6 from the correlation with C-6. The other ^{13}C signals (74.2, 73.9, 72.8 and 72.0 p.p.m.) were therefore determined to be the allyl methylene carbons (C-1′). As the other methine carbons (C-2, -3, -4 and -5) were not specifically assigned by the C-H correlated spectroscopy, H-H correlated spectroscopy, which can investigate the correlation between two protons bound to two adjacent carbon atoms, was examined (Figure 4). The ^{1}H signal at 3.38 p.p.m. was assigned to H-2 from the correlation to H-1 at 5.15 p.p.m. Subsequently, the ^{1}H signal at 3.71 p.p.m. was assigned to H-3 from the correlation to H-2. In a similar manner, the ^{1}H signals at 3.45, 4.05 and 3.65–3.52 p.p.m. were stepwise assigned to H-4, -5 and -6, respectively. Finally, the ^{13}C signals at 81.2, 79.2, 77.5 and 70.7 p.p.m. were assigned to C-3, -2, -4 and -5 from their correlation to H-3, -2, -4 and -5 (Figure 3). The proposed ^{1}H- and ^{13}C assignments for A8T were confirmed by the heteronuclear multiple bond correlation spectrum, which provides correlations between carbons and protons that are separated by two and three bonds (Supplementary Figure 1). Although the spectral pattern of A6T was similar to that of A8T, the whole signals became very broad owing to the presence of a complex mixture of compounds with different allylation degrees and substitution positions (Figure 2). However, the degrees of allylation for both A6T and A8T were calculated from the integral ratios of H-2′ and H-3, -6, -4 and -2. The degrees of allylation measured by the ^{1}H-NMR method for A6T and A8T were 5.99 and 7.51, respectively, which were in agreement with the feed molar ratio of trehalose and allyl bromide. MALDI-TOF-MS analysis of A8T was performed to confirm the validity of the allylation degree measured by the ^{1}H-NMR method. The peaks at *m*/*z* 189 and 378 were ascribed to CHCA (matrix) and 2CHCA, respectively. The molecular weight of an ideal A8T ($C_{36}H_{54}O_{11}$) is 662.37. The peaks at *m*/*z* 892, 851, 703 and 685 were ascribed to A8T + Na + H_2O + CHCA, A8T + CHCA, A8T + Na + H_2O and A8T + Na, respectively (Figure 5). The peak at *m*/*z* 646 was ascribed to A7T ($C_{33}H_{50}O_{11}$ = 622.34) + Na + H^+. The MALDI-TOF-MS data indicated that the isolated A8T mainly contained allylated compounds with 8.0 and 7.0 of allylation degrees, a finding that is in agreement with the ^{1}H-NMR spectroscopy results.

Characterization and properties of A*x*T-S4P and A*x*T-S3I

The obtained A*x*T (x = 6 or 8) was crosslinked with S4P or S3I by thiol-ene photopolymerization at an allyl/thiol ratio of 1:1 to yield a A*x*T-S4P or A*x*T-S3I film. Figure 6 shows the photographs of the generated A*x*T-S4P and A*x*T-S3I films. All of the films were transparent and pale yellow, indicating that no phase separation of the two components occurred. The A6T-based films were of a slightly deeper yellow color than the A8T-based films. All of the films exhibited a relatively high transparency to visible light, as is obvious from Figure 7. Additionally, the S3I-based films were more flexible than the S4P-based films.

Figures 8 and 9 show the Fourier transform infrared spectroscopy (FT-IR) spectra of A*x*T-S4P and A*x*T-S3I compared with those of A*x*T, S4P and S3I. A6T and A8T exhibited absorption bands at 1643 cm^{-1} and 991, 918 cm^{-1}, which are characteristic of allyl groups and are ascribed to C=C stretching and =C-H out-of-plane bending vibrations, respectively. The absorption bands at 918 and 1643 cm^{-1} that are characteristic of allyl groups were almost nonexistent for A*x*T-S4P and A*x*T-S3I. The other band at 991 cm^{-1}, which is characteristic of the allyl groups of A*x*T, could not be used to monitor the progression of the thiol-ene reaction

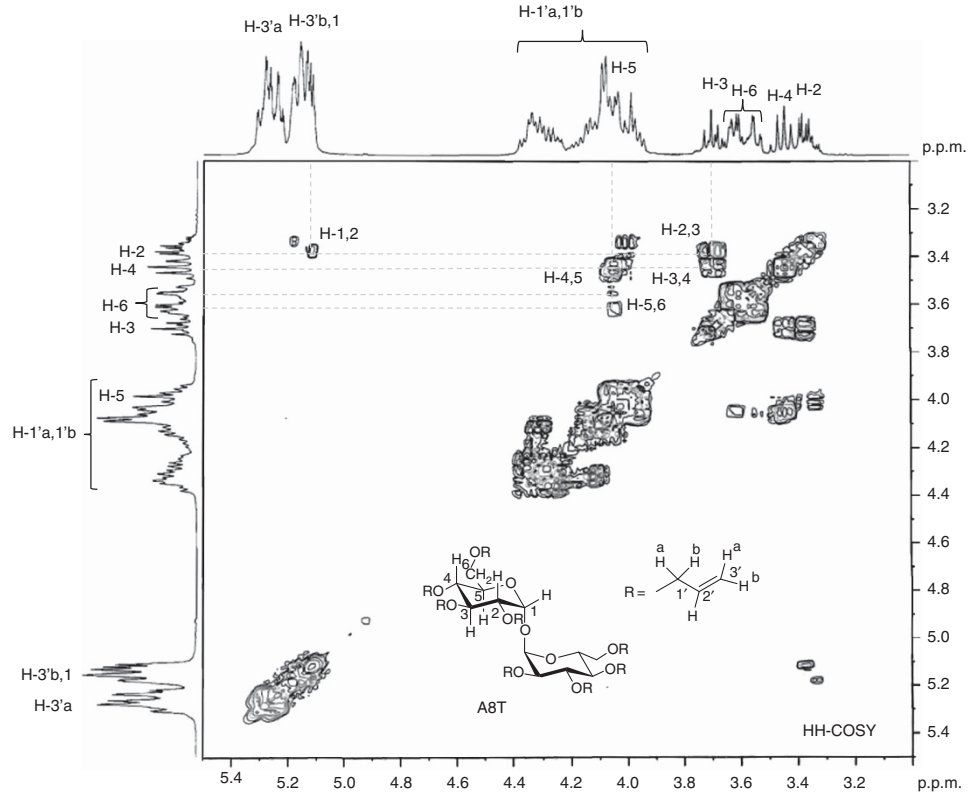

Figure 4 Two-dimensional H-H correlated spectroscopy (2D HH-COSY) spectrum of A8T in $CDCl_3$.

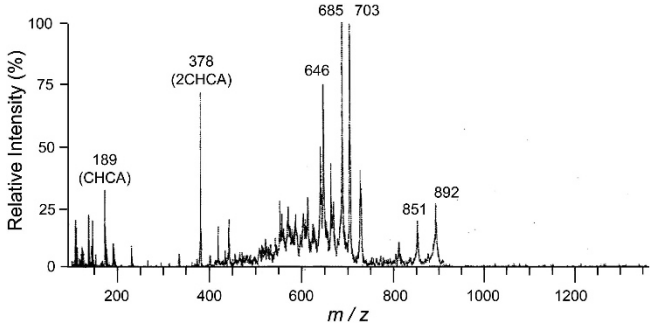

Figure 5 Matrix-assisted laser desorption ionization time-of-flight (MALDI-TOF) mass spectrum of A8T.

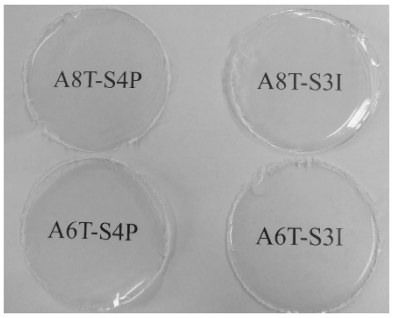

Figure 6 Photographs of A8T-S4P, A8T-S3I, A6T-S4P and A6T-S3I films. A full color version of this figure is available at *Polymer Journal* online.

because the band overlapped with another band at 995 cm^{-1} for S4P and S3I. Additionally, the absorption band at *ca.* 2570 cm^{-1} related to S–H stretching vibration in S4P and S3I almost completely disappeared after the reaction, even in the enlarged FT-IR spectra of A*x*T-S4P and A*x*T-S3I. These results suggest that the thiol-ene photopolymerization of the thiol group of S4P or S3I and allyl group of A*x*T smoothly proceeded. Regarding the absorption band due to O–H stretching vibration, the observation of a very weak and broad band at approximately 3495 cm^{-1} for A8T suggests that A8T contains a small amount of hydroxy groups that were not completely allylated, which is in agreement with the results from ^{1}H-NMR and MALDI-TOF-MS. In contrast, A6T exhibited a clear band at approximately 3471 cm^{-1} owing to the hydrogen-bonded hydroxy group, which possesses a value lower than that of free hydroxy groups ($\sim$3650–3585 cm^{-1}). Additionally, bands due to hydrogen-bonded hydroxy groups were observed at 3440 and 3485 cm^{-1} for A6T-S4P and A6T-S3I, respectively. These results suggest that there are intermolecular hydrogen bonding interactions for A6T, A6T-S4P and A6T-S3I.

Table 1 summarizes the T_g's that were determined from the second heating DSC thermograms of A*x*T-S4P and A*x*T-S3I (Supplementary Figure 2). No melting endothermal peak was observed in the DSC thermograms, indicating that all the samples are amorphous. A6T-S4P, A6T-S3I and A8T-S4P demonstrated similar T_g values (27–28 °C), whereas the T_g (11.2 °C) of A8T-S3I was a little lower than those of the other samples. Although we anticipated that A8T would yield a cured resin with a higher T_g than A6T because of the higher allylation degree of A8T, the A6T-based cured resin actually demonstrated a slightly higher T_g than the A8T-based cured resin did. This result may be attributed to the contribution of hydrogen bonding interactions of the residual hydroxy groups of A6T. For

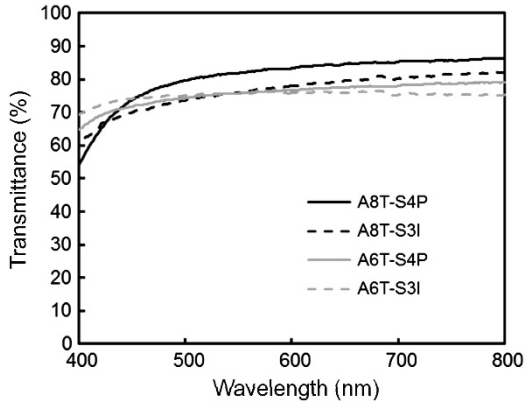

Figure 7 Ultraviolet–visible (UV–vis) spectra of A8T-S4P, A8T-S3I, A6T-S4P and A6T-S3I films with a thickness of 0.5 mm.

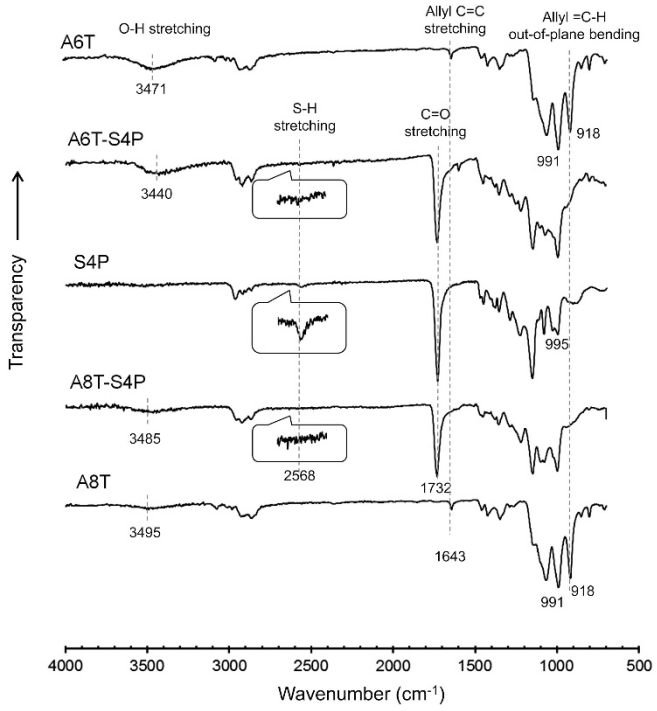

Figure 8 Fourier transform infrared spectroscopy (FT-IR) spectra of A6T, A6T-S4P, S4P, A8T-S4P and A8T.

thermally cured vinylbenzyl-etherified trehalose, a similar decrease in the T_g with an increasing degree of substitution has been reported by our group.[13] Additionally, S3I did not produce a cured resin with a higher T_g than S4P did, most likely due to the lower functionality of S3I, despite the presence of a heat-resistant isocyanurate moiety. Table 1 also summarizes the T_5's obtained from the thermogravimetric analysis curves of A*x*T-S4P and A*x*T-S3I (Supplementary Figure 3). A8T-based cured samples exhibited higher T_5 than A6T-based cured samples did, indicating that hydroxy-containing sugar units possess relatively low heat resistance. The A8T-S4P was thermally more stable than the polymer network prepared by the thiol-ene photopolymerization of diallylsucrose (A2S) and tetrakis(3-mercaptopropionate) (PETKMP), which begin to decompose from ~230 °C.[19]

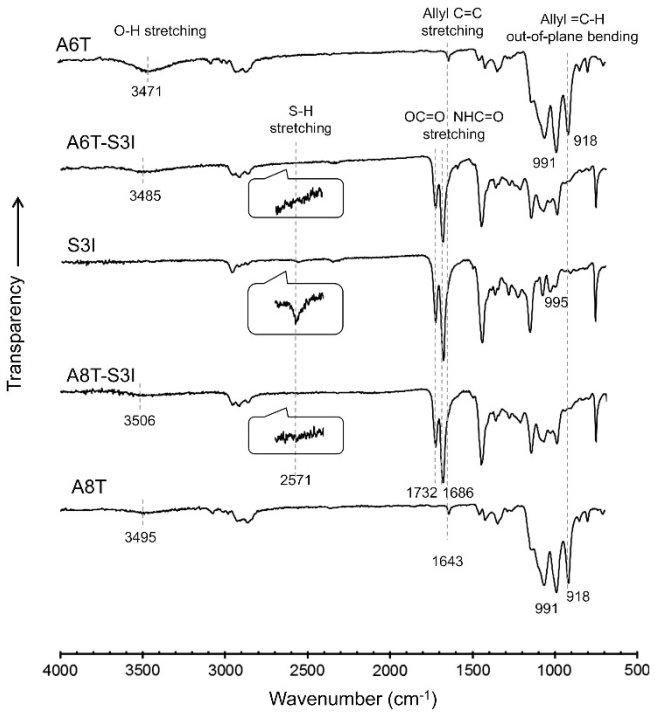

Figure 9 Fourier transform infrared spectroscopy (FT-IR) spectra of A6T, A6T-S3I, S3I, A8T-S3I and A8T.

Table 1 T_g's measured by DSC and T_5's measured by TGA for A6T-S4P, A6T-S3I, A8T-S4P and A8T-S3I

Sample	T_g (°C)	T_5 (°C)
A6T-S4P	28.4	289.4
A6T-S3I	27.4	275.6
A8T-S4P	27.6	251.4
A8T-S3I	11.2	256.1

Abbreviations: DSC, differential scanning calorimetry; T_g, glass transition temperature; TGA, thermogravimetric analysis.

Figure 10 shows the DMA curves of A*x*T-S4P and A*x*T-S3I. The tan δ peak temperatures of A8T-S4P and A6T-S4P (36.7 °C and 36.8 °C, respectively) were higher than those of A8T-S3I and A6T-S3I (21.9 °C and 23.2 °C, respectively). Although a similar trend was observed for the T_g measured by DSC, the difference between the samples was more prominent in the tan δ peak temperature by DMA measurement. This result may be related to the increased functionality of S4P relative to S3I, which leads to the production of cured resins with a higher crosslinking density. Additionally, the tan δ peak temperature of A6T-based films was slightly higher than that of the A8T-based films, which is in agreement with the DSC results. A2S-PETKMP, which contains a greater hydroxy content than A6T-S4P, has been reported to exhibit a higher tan δ peak temperature (58 °C) than A6T-S4P (36.8 °C).[19] The storage modulus (E') at a rubbery plateau region is known to be related to the crosslinking density of the cured resin.[25] The descending order for E' at the rubbery plateau region at approximately 50 °C was A8T-S4P > A6T-S4P > A8T-S3I (> A6T-S3I), given that the DMA measurement for A6T-S3I automatically stopped at approximately 40 °C because the sample became very soft. This order is in good

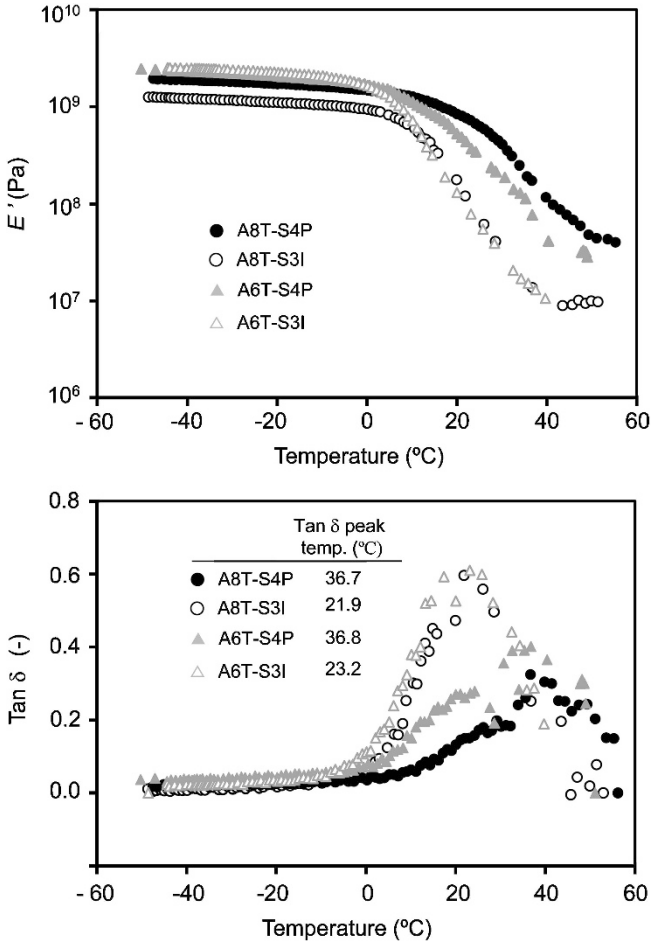

Figure 10 Dynamic mechanical analysis (DMA) curves of A8T-S4P, A8T-S3I, A6T-S4P and A6T-S3I.

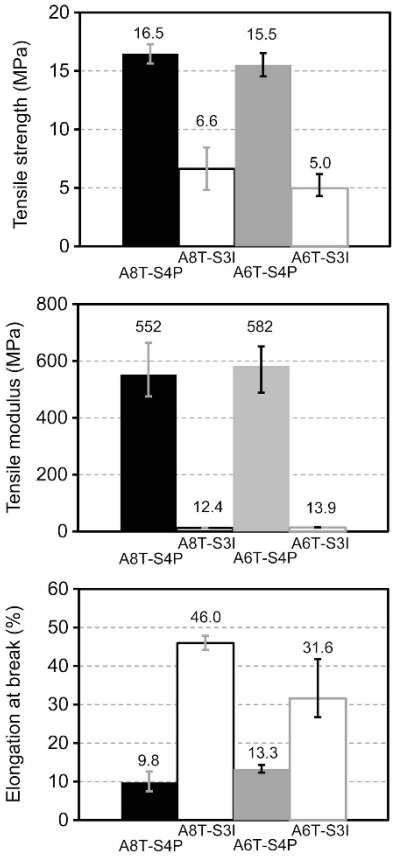

Figure 11 Tensile properties of A8T-S4P, A8T-S3I, A6T-S4P and A6T-S3I.

agreement with the results expected from the polymer network structure that is formed after curing. In contrast, the descending order for E' in the glassy state at the temperature region from $-40\,^{\circ}C$ to $-20\,^{\circ}C$ was A6T-S3I ≈ A6T-S4P > A8T-S4P > A8T-S3I, suggesting that hydrogen bonding interactions are more important than the crosslinking density.

Figure 11 shows the tensile properties of the photo-cured resins at room temperature. The S4P-based films demonstrated a much higher tensile strength and modulus than the S3I-based films did. This result is attributed to the fact that the S4P-based films possessed a tan δ peak temperature higher than room temperature (approximately 25 °C), whereas the tan δ peak temperature of the S3I-based films was lower than the room temperature. Actually, the tensile modulus at room temperature was close to the E' at approximately 25 °C. The S3I-based films, which were in a rubbery state at room temperature, exhibited a much higher elongation at break than the S4P-based films did. However, there was not much difference in the tensile properties of A8T- and A6T-based films.

CONCLUSIONS

The structure of A*x*T ($x = 6$ or 8) prepared by the reaction of trehalose and allyl bromide was fully characterized by two-dimensional NMR and FT-IR spectroscopy. Thiol-ene photopolymerization of A*x*T with S4P or S3I at a allyl/thiol ratio of 1:1 produced A*x*T-S3I or A*x*T-S4P. All of the photo-cured films exhibited high transparency to visible light. The A6T-based films demonstrated a slightly higher T_g, as measured by DSC, and tan δ peak temperature, as measured by DMA, than the A8T-based films did, indicating that the thermal molecular motion of the polymer chain is more restricted by the hydrogen bonding of the residual hydroxy group of the trehalose moiety than by crosslinking via the sulfide bond. The T_g and tan δ peak temperature of the S4P-based films were higher than those of the S3I-based films, reflecting a difference in the crosslinking density. Additionally, the S4P-based films exhibited much higher tensile strength and modulus at room temperature than S3I-based films did. The T_5 of A8T-based films was much higher than that of A6T-based films.

1 Newman, Y. M., Ring, S. G. & Colaco, C. The role of trehalose and other carbohydrates in biopreservation. *Biotechnol. Genet. Eng. Rev.* **11,** 263–294 (1993).
2 Paiva, C. L. & Panek, A. D. Biotechnological applications of the disaccharide trehalose. *Biotechnol. Annu. Rev.* **2,** 293–314 (1996).
3 Richards, A. B., Krakowka, S., Dexter, L. B., Schmid, H., Wolterbeck, A. P. M., Waalkens-Berendsen, D. H., Shigoyuki, A. & Kurimoto, M. Trehalose: a review of properties, history of use and human tolerance, and results of multiple safety studies. *Food Chem. Toxicol.* **40,** 871–898 (2002).
4 Elbein, A. D., Pan, Y. T., Pastuszak, I. & Carroll, D. New insights on trehalose: a multifunctional molecule. *Glycobiology* **13,** 17R–27R (2003).
5 Teramoto, N., Sachinvala, N. D. & Shibata, M. Trehalose and trehalose-based polymers for environmentally benign, biocompatible and bioactive materials. *Molecules* **13,** 1773–1816 (2008).
6 Higashiyama, T. Novel functions and applications of trehalose. *Pure Appl. Chem.* **74,** 1263–1270 (2002).
7 Teramoto, N., Arai, Y., Shibasaki, Y. & Shibata, M. A facile synthesis of a novel polyacetal containing trehalose residue in the main chain. *Carbohydrate Polym.* **56,** 1–6 (2004).

8 Kukowka, S. & Maślińska-Solich, J. S. α,α-Trehalose-based polyacetals and macrocyclic acetals. *Carbohydrate Polym.* **80,** 711–719 (2010).
9 Teramoto, N., Unosawa, M., Matsushima, S. & Shibata, M. Synthesis and properties of thermoplastic alternating copolymers containing trehalose and siloxane units by hydrosilylation reaction. *Polym. J.* **39,** 975–981 (2007).
10 Teramoto, N., Arai, Y. & Shibata, M. Thermo-reversible Diels-Alder polymerization of difurfurylidene trehalose and bismaleimides. *Carbohydrate Polym.* **64,** 78–84 (2006).
11 Srinivasachari, S., Liu, Y., Prevette, L. E. & Reineke, T. M. Effect of trehalose click polymer length on pDNA complex stability and delivery efficacy. *Biomaterials* **28,** 2885–2898 (2007).
12 Eissa, A. M. & Khosravi, E. Synthesis of a new smart temperature responsive glycopolymer via click-polymerization. *Eur. Polym. J.* **47,** 61–69 (2011).
13 Teramoto, N. & Shibata, M. Trehalose-based thermosetting resins—1. Synthesis and thermal properties of trehalose vinylbenzyl ether. *J. Appl. Polym. Sci.* **91,** 46–51 (2004).
14 Morgan, C. R., Magnotta, F. & Ketley, A. D. Thiol/ene photocurable polymers. *J. Polym. Sci. Polym. Chem. Ed.* **15,** 627–645 (1977).
15 Hoyle, C. E., Lee, T. Y. & Roper, T. Thiol-enes: chemistry of the past with promise for the future. *J. Polym. Sci. Part A* **42,** 5301–5338 (2004).
16 Dondoni, A. The emergence of thiol-ene coupling as a click process for materials and bioorganic chemistry. *Angew. Chem. Int. Ed.* **47,** 8995–8997 (2008).
17 Nilsson, C., Simpson, N., Malkoch, M., Johansson, M. & Malmström, E. Synthesis and thiol-ene photopolymerization of allyl-ether functionalized dendrimers. *J. Polym. Sci. Part A* **46,** 1339–1348 (2008).
18 Lowe, A. B. Thiol-ene 'click' reactions and recent applications in polymer and materials synthesis. *Polym. Chem.* **1,** 17–36 (2010).
19 Ortiz, R. A., Martinez, A. Y. R., Valdéz, A. E. G. & Duarte, M. L. B. An effective method to prepare sucrose polymers by thiol-ene photopolymerization. *Carbohydrate Polym.* **78,** 282–286 (2009).
20 Ortiz, R. A., Martinez, A. Y. R., Valdéz, A. E. G. & Duarte, M. L. B. Preparation of a crosslinked sucrose polymer by thiol-ene photopolymerization using dithiothreitol as comonomer. *Carbohydrate Polym.* **82,** 822–828 (2010).
21 Sangermano, M., Colucci, G., Fragale, M. & Rizza, G. Hybrid organic–inorganic coatings based on thiol-ene systems. *React. Funct. Polym.* **69,** 719–723 (2009).
22 Vilén, E. M. & Sandström, C. NMR study on the interaction of trehalose with lactose and its effect on the hydrogen bond interaction in lactose. *Molecules* **18,** 9735–9754 (2013).
23 Fukazawa, Y. Investigation of trehalose in water splution by PMR. *Kenkyu Hokoku-Kanagawa-Ken Kogyo Shikenjo* **65,** 42–46 (1994).
24 National Institute of Advanced Industrial Science and Technology (AIST). SDBS/RIO-DB/AIST, Spectral Database for Organic Compounds (SDBS). Available at: http://sdbs.db.aist.go.jp/sdbs/cgi-bin/direct_frame_top.cgi (last accessed 11 April 2014).
25 Taguet, A., Ameduri, B. & Dufresne, A. Crosslinking and characterization of commercially available poly(VDF-co-HFP) copolymers with 2,4,4-trimethyl-1,6-hexanediamine. *Eur. Polym. J.* **42,** 549–2561 (2006).

Supplementary Information accompanies the paper on Polymer Journal website (http://www.nature.com/pj)